A&A, 694, L9 (2025)
https://doi.org/10.1051/0004-6361/202453274

Astronomy & Astrophysics

LETTER TO THE EDITOR

Populations of neutron star ultraluminous X-ray sources

Mind your *b*s and *B*s

Konstantinos Kovlakas[1,2,⋆], Devina Misra[3], Roberta Amato[4], and Gian Luca Israel[4]

[1] Institut d'Estudis Espacials de Catalunya (IEEC), Edifici RDIT, Campus UPC, 08860 Castelldefels (Barcelona), Spain
[2] Institute of Space Sciences (ICE, CSIC), Campus UAB, Carrer de Magrans, 08193 Barcelona, Spain
[3] Department of Physics, Norwegian University of Science and Technology, NO-7491 Trondheim, Norway
[4] INAF – Osservatorio Astronomico di Roma, via Frascati 33, I-00078 Monte Porzio Catone, Italy

Received 3 December 2024 / Accepted 15 January 2025

ABSTRACT

Ultraluminous X-ray sources (ULXs) with neutron star (NS) accretors pose a challenge to traditional accretion models, sparking a debate regarding the role of geometrical beaming and strong magnetic fields (B). The reduction of the Thomson cross-section in the presence of strong B leads to a modification of the Eddington limit; therefore, it is expected to affect significantly the observational appearance of NS-ULXs. We investigate the role of this modification using population synthesis models and explore its effects on the X-ray luminosity functions, spin-up rates, and outflow energetics of the observed NS-ULXs. Our results show that the new prescription allows NS-ULXs to achieve super-Eddington luminosities with a milder beaming compared to before, improving the agreement with observations. In addition, it broadens the range of spin-up rates, allowing for more diverse conditions in NS-ULXs in terms of accretion rates and magnetic fields. More importantly, the reduced beaming increases the likelihood of observing the NS-ULXs within wind-powered nebulae, such as NGC 5907 ULX-1. Our findings highlight the need to take B effects into account, independently of the usual approach based on geometrical beaming or strong B. Finally, we call for magnetospheric accretion prescriptions that can be integrated in population synthesis codes.

Key words. accretion, accretion disks – magnetic fields – stars: black holes – stars: evolution – stars: neutron – X-rays: binaries

1. Introduction

Ultraluminous X-ray sources (ULXs) are accreting compact objects, distinct from active galactic nuclei, with luminosities ranging from 10^{39} to $10^{42}\,\mathrm{erg\,s^{-1}}$ (e.g., Kaaret et al. 2017; King et al. 2023). Based on the Eddington limit and assuming pure hydrogen material, we have

$$L_{\rm Edd} = 1.26\times10^{38}\,\mathrm{erg\,s^{-1}}\,M_1, \tag{1}$$

where M_1 is the mass of the accretor in solar units ($M_\odot$), ULXs could represent accreting black holes (BHs) with $M_1 \sim 10$–10^4. However, their association with star-forming regions suggests they are X-ray binaries (e.g., Zezas et al. 2002), where accretors tend to have lower masses ($\lesssim$20 $M_\odot$; Miller-Jones et al. 2021). Consequently, the majority of ULXs are now thought to be super-Eddington accretors.

The Shakura & Sunyaev (1973) model for super-critical accretion onto BHs, where the mass-transfer rate $\dot{M}_{\rm tr}$ exceeds the Eddington rate $\dot{M}_{\rm Edd}$, describes an accretion disk that is locally Eddington-limited at all radii and becomes geometrically thick near the accretor. This model predicts strong outflows, and a bolometric luminosity higher than the $L_{\rm Edd}$ value,

$$L_{\rm bol} = L_{\rm Edd}\begin{cases}1+\ln\dot{m} & \dot{m}>1,\\ \dot{m} & \dot{m}\le 1,\end{cases} \tag{2}$$

where $\dot{m} = \dot{M}_{\rm tr}/\dot{M}_{\rm Edd}$ is the Eddington ratio and $L_{\rm Edd} = 0.1\dot{M}_{\rm Edd}c^2$, adopting accretion efficiency 0.1 (Frank et al. 2002; for completeness, the sub-Eddington regime, $\dot{m} < 1$, is also included). We note that Eq. (2) does not take into account the role of advection (e.g., Beloborodov 1998; Chashkina et al. 2019), which may decrease the bolometric luminosity by a factor of ∼30–40% (e.g., Lipunova 1999; Poutanen et al. 2007). Still, luminosities of $\gtrsim 10^{40}\,\mathrm{erg\,s^{-1}}$ cannot be accounted for by the $\ln\dot{m}$ term. Instead, they are better explained by the collimation of the radiation escaping through a funnel formed by the outflows (King et al. 2001). As a result, the observed luminosity under the isotropic emission, $L_{\rm iso}$, is

$$L_{\rm iso} = b^{-1}L_{\rm bol}, \tag{3}$$

where the beaming factor, b, represents the fraction of the full solid angle through which radiation escapes. Here, b is known to be correlated with $\dot{m}$ (King 2009),

$$b = \begin{cases}1 & \dot{m}\le 8.5,\\ (8.5/\dot{m})^2 & \dot{m}>8.5\end{cases} \tag{4}$$

allowing for extreme luminosities without invoking extreme BH masses (e.g., $10^{42}\,\mathrm{erg\,s^{-1}}$ for $M_1 = 30$ and $\dot{m} = 60$).

The discovery of pulsating ULXs (PULXs; Bachetti et al. 2014) confirmed the existence of neutron star (NS) ULXs, often exhibiting highly super-Eddington luminosities. The most extreme example, NGC 5907 ULX-1, reached $L_{\rm iso}/L_{\rm Edd} \sim 1000$ (Israel et al. 2017) and, under the beaming scenario, this corresponds to small $b < 10^{-2}$. Such low b values are inconsistent with the sinusoidal profiles in PULXs (e.g., Kaaret et al. 2017) and have not been reproduced via numerical simulations (e.g., Abarca et al. 2021). This has prompted investigations into alternative scenarios, primarily focusing on the role of the "usual suspect" in NSs, namely: the magnetic field (e.g., Eksi et al. 2015).

⋆ Corresponding author; kovlakas@ice.csic.es

In the presence of strong magnetic fields, the Thomson cross-section is reduced for photon energies below the cyclotron energy (Herold 1979), increasing the Eddington limit to a critical luminosity (e.g., Paczynski 1992; Dall'Osso et al. 2015; Brightman et al. 2018) of

$$L_{\rm crit} \approx 2B_{12}^{4/3} L_{\rm Edd}, \quad (5)$$

where B_{12} is the dipolar magnetic field in units of 10^{12} G. Consequently, NS-ULXs could be sub-Eddington accretors with $B_{12} \sim 10{-}1000$ without beamed emission. However, this interpretation relies on highly magnetised NSs, which could push many PULXs in the propeller regime, where infalling matter is expelled rather than accreted.

Whether the observational appearance of PULXs can be explained by beaming or extreme Bs is a matter of debate since their discovery. Arguments in favour of the beaming are: (i) the high-B scenario requires $B_{12} \gtrsim 100$ (e.g., Lasota & King 2023), higher than the typical values in X-ray binaries and constraints in PULXs (e.g., Walton et al. 2018; Middleton et al. 2019); (ii) collimated emission in NS-ULX simulations (e.g., Mushtukov et al. 2019; Inoue et al. 2023) and its consequences for the spectra of ULXs (e.g., Poutanen et al. 2007; King 2009); (iii) the extension of the X-ray luminosity function (XLF) to the ULX regime, reproduced by population synthesis studies employing beaming, in star-forming galaxies (e.g., Misra et al. 2023), including BH-dominated low-metallicity galaxies (e.g., Wiktorowicz et al. 2019), and in NS-dominated passive galaxies agreeing with ULX demographic studies (e.g., Kovlakas et al. 2020).

Conversely, the high-B scenario ($B_{12} \gtrsim 100$) has been supported by the following points: (i) expanding nebulæ near ULXs have been found to require mechanical power, in terms of outflow kinetic power ($L_{\rm kin}$), similar to the observed luminosity of the ULXs (e.g., Holmberg II X-1; Pakull & Mirioni 2002). This suggests that the inferred luminosities are not overestimated due to strong beaming (e.g., $L_{\rm kin} \sim 1.3 \times 10^{41}$ erg s^{-1} in NGC 5907 ULX-1; Belfiore et al. 2020); (ii) the orbital decay observed in M82 X-2 points at $\dot{M}_{\rm tr} \gg \dot{M}_{\rm Edd}$, while the mass available to the accretor is sufficient to explain its luminosity (e.g.; Bachetti et al. 2022, however, also see King & Lasota 2021), as well as mild beaming hinted by the long-term spin-down rate of the system (Liu 2024); (iii) extreme beaming implies a large population of hidden ULXs, challenging to reproduce in population synthesis models which often force a b limit (e.g., >0.0032; Wiktorowicz et al. 2019; Misra et al. 2023); and (iv) strong beaming precludes the detection of pulsations due to the reflections of X-ray photons in a geometrically thick inner accretion wall (e.g., Mushtukov et al. 2021; Mushtukov & Portegies Zwart 2023).

It has been suggested that the observational appearance of PULXs may be explained by the combined effect of B on $L_{\rm Edd}$, the presence of multipolar components, and moderate beaming (e.g., Israel et al. 2017; Erkut et al. 2020). To date, however, there has been no comprehensive prescription devised for the magnetic field configuration of NSs and magnetospheric accretion that would be applicable to both sub-Eddington and super-Eddington regimes. Consequently, the models of Shakura & Sunyaev (1973), Poutanen et al. (2007), King (2009) are commonly employed in observational (e.g., Middleton et al. 2019) and theoretical studies (e.g., Lasota & King 2023), as well as in population synthesis models (e.g., Wiktorowicz et al. 2019; Misra et al. 2023, 2024).

In this Letter, we evaluate whether the combination of the modified $L_{\rm Edd,B}$ and beaming reconciles the observations discussed above, using population synthesis models. Finally, we highlight the importance of integrating in the models up-to-date magnetospheric accretion prescriptions towards a self-consistent framework for the study of NS-ULXs.

2. Methodology

In the following paragraphs, we describe the calculation of the observable quantities ($L_{\rm iso}$, $L_{\rm kin}$, $\dot{\nu}$) in simulated systems, as well as the setup of our population synthesis models.

2.1. Observables

The B-dependent critical luminosity acts as a new Eddington limit, only if $L_{\rm crit} > L_{\rm Edd}$ (Paczynski 1992):

$$L_{\rm Edd,B} = \max\left\{1, 2B_{12}^{4/3}\right\} L_{\rm Edd}, \quad (6)$$

by combining Eqs. (1) and (5). Then, Eqs. (1)–(4) are applied to estimate the apparent luminosity, $L_{\rm iso}$, for both BHs and NSs, but now the $\dot{m}$ value is determined relative to the $L_{\rm Edd,B}$ for NSs.

The mechanical feedback ($L_{\rm kin}$) is challenging to model due to its dependence on the outflow rate and speed, both of which vary as functions of the launching radius. This distribution is shaped by the accretion geometry and $\dot{M}_{\rm tr}$. To estimate $L_{\rm kin}$ at an order-of-magnitude level, we assume that matter is accreted at approximately the Eddington rate (however it can exceed it by a factor of 6 in NSs; Basko & Sunyaev 1976; Kaaret et al. 2017), while the rest of the transferred mass is expelled with speed $\approx 0.2\,c$ (e.g., Pinto et al. 2016):

$$L_{\rm kin} \approx \frac{1}{2}\left(\dot{M}_{\rm tr} - \dot{M}_{\rm Edd}\right)(0.2\,c)^2 = \frac{\dot{m}-1}{5} L_{\rm Edd}. \quad (7)$$

The spin-up rate $\dot{\nu}$ in NSs is the result of the torque from the accreted material at rate $\dot{M}$ (at $R_{\rm M}$):

$$\dot{\nu} = \frac{\dot{M}\,(GMR_{\rm M})^{1/2}}{2\pi I}, \quad (8)$$

where $I \approx 10^{45}$ g cm^2 is the moment of inertia. Here, $R_{\rm M}$ is the magnetospheric radius,

$$R_{\rm M} = \left(\frac{\mu^4}{2GM\dot{M}^2}\right)^{1/7}, \quad (9)$$

where $\mu = BR^3$ is the magnetic moment with dipolar field, B, and radius, R. On this basis, we get

$$R_{\rm M} = 3.24 \times 10^8\ \dot{M}_{17}^{-2/7} M_1^{-1/7} B_{12}^{4/7} R_6^{12/7}\ {\rm cm}, \quad (10)$$

$$\dot{\nu} = 3.30 \times 10^{-12}\ \dot{M}_{17}^{6/7} M_1^{-3/7} B_{12}^{2/7} R_6^{6/7}\ {\rm s}^{-2}, \quad (11)$$

where the accretion rate, $\dot{M}_{17}$ (at $R_{\rm M}$), magnetic field, B, radius, R_6, and mass, M_1, are in units of 10^{17} g s^{-1}, 10^{12} G, 10^6 cm, and $1\,M_\odot$, respectively. We notice that Eq. (10) is consistent with Shapiro & Teukolsky (1983), but with a larger scaling than the expressions in King et al. (2017) and Lasota & King (2023), as well as a typo in the exponent of the mass term in the latter.

2.2. Population synthesis models

The $L_{\rm Edd}$ corresponding to characteristic masses of compact objects in X-ray binaries may manifest as breaks in XLFs (e.g., Kaaret et al. 2017). Moreover, beaming "carves" the XLFs near these limits and extends them, by shifting the portion of the population that is beamed towards the line of sight to higher luminosities, while concealing the rest. As a result, beaming prescriptions

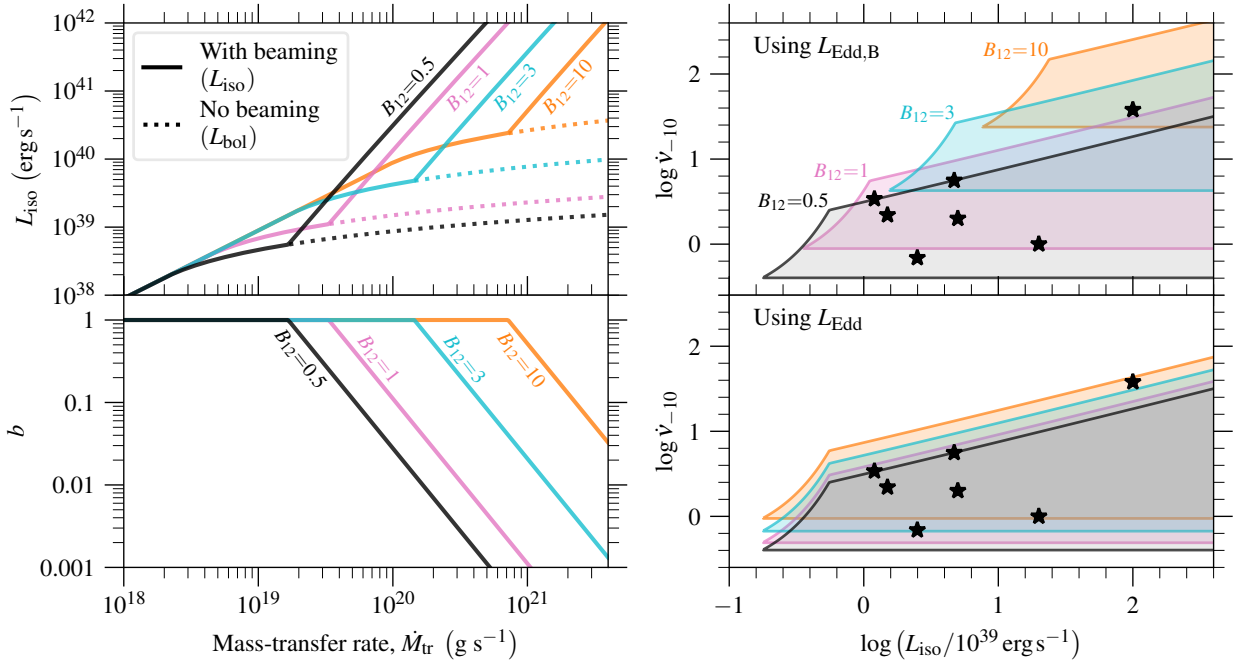

Fig. 1. Effects of beaming and $L_{Edd,B}$ for a 1.4 $M_\odot$ NS of varying B (see coloured text) on the apparent luminosity L_{iso} (upper left), with and without beaming (solid and dotted lines, respectively), and b (bottom left) as a function of the $\dot{M}_{tr}$. We also compare the $\dot{\nu}$ ranges (accretion rate between $\dot{M}_{Edd}$ and $\dot{M}_{tr}$) as a function of the L_{iso} using the modified (upper right) and classical (lower right; increasing B from bottom to top) L_{Edd} against the values of observed PULXs (asterisks; King & Lasota 2019).

can be tested at the population level by comparing population synthesis models with observed XLFs in star-forming galaxies (all PULXs have been found in spiral galaxies; King et al. 2023).

Different codes and choices of stellar evolution parameters can influence the NS/BH ratio, mass-transfer rates, and so on, leading to varying XLF predictions. Here, our goal is not to constrain these parameters, but, rather, to explore the effects of beaming and $L_{Edd,B}$, while ensuring that the results are not an artifact of the specific modelling choices. For this reason, we employed two drastically different approaches: (i) a parametric binary population synthesis code, `COSMIC` v.3.4.17 (Breivik et al. 2020), using the default stellar evolution parameters, and (ii) `POSYDON` v.1 (Fragos et al. 2023), which incorporates up-to-date physics and detailed stellar tracks with `MESA` (Paxton et al. 2011), using parameters reproducing the XLF (cf., model 44 in Misra et al. 2023, 2024). We evolved 10^7 massive binaries in a constant 100 Myr star-formation scenario and selected systems with $\dot{M}_{tr}$ larger than 1% of the classical L_{Edd} to ensure that the full ULX population would be included in the samples (including sub-Eddington ULXs with massive BHs). Focusing on the shape, rather than the normalisation, of the XLFs, we scaled the populations to match the measured scaling of ULXs with star formation rate (~0.5 ULXs per 1 $M_\odot$ yr^{-1}; Kovlakas et al. 2020; Lehmer et al. 2021). Since `POSYDON` does not evolve the magnetic field of NSs, we sampled B values from the resulting distribution in the `COSMIC` population: $\log(B/1\,\mathrm{G}) \sim \mathcal{N}(12.22, 0.64)$ with a maximum at 13.79. This distribution is consistent with the expectation that PULXs are high-mass X-ray binaries with ages that are shorter than the B-decay timescale (e.g., Revnivtsev & Mereghetti 2016).

3. Results

In the left panels of Fig. 1, we show the L_{iso} (upper panel) and b (lower panel) as a function of the $\dot{M}_{tr}$, for $M_1 = 1.4$, and various values of B_{12}. We omit showing the effect of NS mass as it is negligible given its small range (~1–2 $M_\odot$). For $B_{12} = 0.5$, the results are numerically equivalent to using the classical L_{Edd}, as the B dependence is activated for $B_{12} > 0.6$ (Eq. (5)). We find that NS-ULXs with moderately high $B_{12} = 10$ can reach luminosities up to 10^{41} erg s^{-1} with mild beaming (>0.1). Without beaming (dashed lines), significantly higher B_{12} is necessary to account for NS-ULXs with $L_{iso} \approx 10^{41}$ erg s^{-1}.

In Eq. (11), $\dot{M}$ is the accretion rate at R_M, making R_M and $\dot{M}$ co-dependent. Therefore, they cannot be calculated without an exact knowledge of the accretion geometry; thus, they can only be constrained via measurements of $\dot{\nu}$ and B. However, we can estimate a conservative range for $\dot{\nu}$ considering $\dot{M}$ values between $\dot{M}_{Edd}$ (the minimum rate for a super-Eddington NS) and $\dot{M}_{tr}$ (the case where all transferred mass is accreted). The right panels of Fig. 1 depict these ranges for $M_1 = 1.4$ and various values of B_{12}, considering the B-dependent (upper) and the classical L_{Edd} (lower). In both cases, the regions do not include spin-up rates corresponding to the propeller regime; that is, R_M is less than the corotation radius adopting the fastest spin observed in PULXs (0.42 s; Fürst et al. 2016) to remain conservative. The points are the measured values from PULXs taken from King & Lasota (2019) and lie within the regions defined by the model using both prescriptions of L_{Edd}.

In Fig. 2, we present the synthetic XLFs, incorporating both BH and NS-ULXs. Employing the B-dependent $L_{Edd,B}$ (blue lines), instead of the classical L_{Edd} (green lines), enhances the contribution of NS-ULXs. This is attributed to the reduced b, which reveals a larger fraction of the systems. The increased presence of NS-ULXs improves the agreement with the observations, despite the difference between the `COSMIC` and `POSYDON`, particularly in the slope at the less-constrained >10^{40} erg s^{-1} regime, where additional processes might be at play (e.g., neutrino energy loss Mushtukov et al. 2018).

In the left panel of Fig. 3, we compare the beaming factors of NS-ULXs ($L_{iso} \in [10^{39}, 10^{42}$ erg s^{-1}) for the classical (green) and B-dependent L_{Edd} (blue), both of the total (dashed

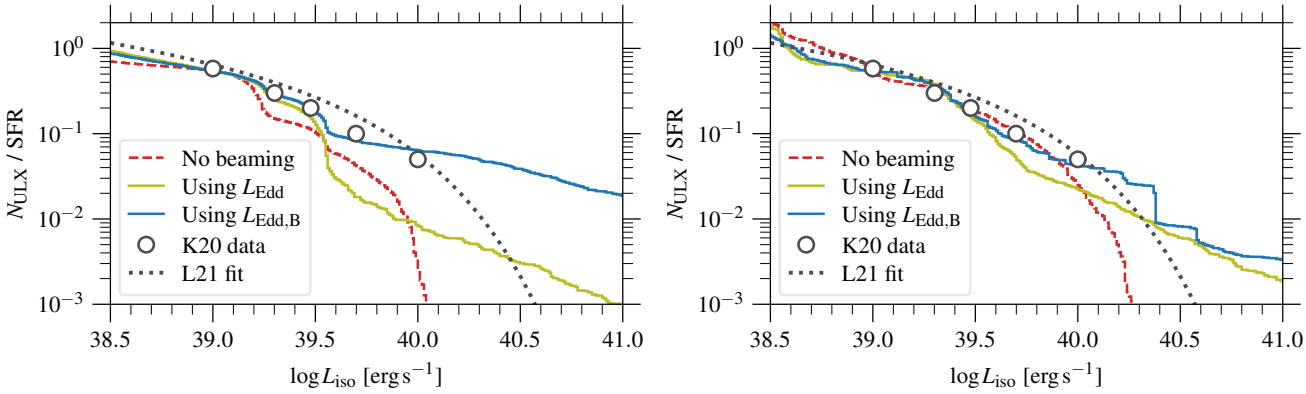

Fig. 2. Synthetic X-ray luminosity functions using `COSMIC` (left) and `POSYDON` (right), in the case of no beaming (red dashed), and beaming with the traditional (green), or modified Eddington limit (blue). The populations include both BH and NS-ULXs, compared against observational constraints from the XLF fit of Lehmer et al. (2021, see L21 in the legend) for nearby solar-metallicity star-forming galaxies (black), and ULX demographic data (open circles) from Kovlakas et al. (2020, see K20 in the legend) using larger galaxy samples (Kovlakas et al. 2021).

curves) and the observed (weighted by b; solid curves) synthetic populations. The classical $L_{\rm Edd}$ implies a highly beamed total population, with a moderately beamed ($b \sim 0.1-0.5$) observed subpopulation with luminosities in the $10^{39}-10^{40}$ erg s^{-1} range (cf. Fig. 1). In contrast, the use of $L_{\rm Edd,B}$ results in more diverse populations. About half of NS-ULXs are moderately beamed ($b \sim 0.05-0.5$), with the rest representing the majority of the observed population with mild beaming ($b > 0.7$) and luminosities spanning the full range of PULXs for $B_{12} \sim 0.5-10$ (cf. Fig. 1).

The order-of-magnitude estimate for the kinetic power of outflows in NS-ULXs can reach up to 10^{42} erg s^{-1}. Depending mainly on the $\dot{M}_{\rm tr}$, it is not affected by the $L_{\rm Edd}$ prescription for the total population (dashed lines in Fig. 3; right panel). However, when we account for the observed fraction of NS-ULXs (not beamed out of the line of sight), the distribution of $L_{\rm kin}$ shifts downward by one and two orders of magnitude using the $L_{\rm Edd,B}$ and $L_{\rm Edd}$, respectively.

4. Discussion

The increased Eddington limit, $L_{\rm Edd,B}$ allows for both sub- and super-Eddington NS-ULXs without beaming, as well as super-Eddington NS-ULXs with milder beaming as B increases (see Appendix A for practical limits and formulæ). This contrasts with the classical $L_{\rm Edd}$ leading to all NS-ULXs being strongly beamed. Interestingly, sub-Eddington NS accretors do not need to exhibit $B_{12} \gtrsim 100$ to explain the PULX luminosities, since for $L_{\rm Edd,B} = 10^{39}-10^{41}$ erg s^{-1}, we have $B_{12} \sim 2-70$.

The effect of the magnetic field in the critical luminosity of NS-ULXs enhances their contribution in the XLFs and helps smooth out prominent breaks (e.g., Kaaret et al. 2017), offering a better match with observed XLFs (e.g., Lehmer et al. 2021) and ULX demographics (e.g., Kovlakas et al. 2020). This has been achieved with magnetic fields in the observed range of X-ray binaries ($B_{12} \sim 0.1-10$). However, since our modelling focuses on the general properties of NS-ULXs and the effects on the XLFs, we did not exclude the possibility of multi-polar component magnetic fields that might be required to explain all observables in individual PULXs (e.g., Israel et al. 2017).

The inferred mechanical power of $L_{\rm kin} \approx 1.3 \times 10^{41}$ erg s^{-1} for the nebula near NGC 5907 ULX-1 (Belfiore et al. 2020) is comparable to the apparent ULX luminosity. This often serves as an argument against beaming, however, it remains uncertain whether the mechanical power must be similar to the bolometric luminosity. Our order-of-magnitude estimates of $L_{\rm kin}$ can reach even higher values, provided high $\dot{M}_{\rm tr}$ values, independently of beaming. More importantly, using the classical $L_{\rm Edd}$ leads to small b, which makes it unlikely to find NS-ULXs close to wind-powered nebulæ. This is evident from the shift of two orders of magnitude in the total and observed distribution in Fig. 3. Conversely, the lower b in the modified $L_{\rm Edd,B}$ results in a shift of only one order of magnitude, increasing the chances of observing such systems as NGC 5907 ULX-1. Systematic searches of wind-powered nebulæ, with or without the detection of the PULXs powering them, can help achieve a measurement for this shift and put constraints on beaming and outflow models of PULXs.

Using the classical $L_{\rm Edd}$ results in a range of $\dot{\nu}$ values that just covers the observed values (Fig. 1; lower right), with half of them indicating spin-up rates close to the maximum possible for $B_{12} \lesssim 10$. This requires either extreme B values or calls for the majority of the transferred mass to reach the magnetospheric radius ($\dot{M} \approx \dot{M}_{\rm tr}$), potentially leading to reduced outflows. In this analysis, we neglected disk-star coupling that might introduce additional angular momentum losses, thereby further reducing the spin-up rate. On the other hand, the B-dependent $L_{\rm Edd,B}$ reduces the $\dot{m}$, shifting both the apparent luminosities and the locus of super-Eddington sources in the diagram, resulting in a broader range of spin-up rates. In this scenario, NS-ULXs may exhibit a wider variety of spin-up behaviours, with moderate B. Discovery of PULXs with higher spin-up rates could rule out the classical $L_{\rm Edd}$ scenario.

We highlight the importance of incorporating a more detailed treatment of the effects of magnetic fields in NS-ULXs, especially with respect to the $L_{\rm Edd}$. In working towards a self-consistent framework of NS-ULXs, we need parameter studies (investigating kick velocity distributions, mass-transfer prescriptions; e.g., El Mellah et al. 2019, and other properties) with population synthesis codes integrating results from magnetospheric accretion simulations. The latter can provide more realistic prescriptions for the bolometric luminosity and b in NS-ULXs (e.g., Vasilopoulos et al. 2021), which are often extrapolated (e.g., Wiktorowicz et al. 2019; Misra et al. 2024) from the BH-ULX population (King 2009), although they are expected to be qualitatively similar (e.g., King et al. 2023). Furthermore, the dependence of $R_{\rm M}$ and $\dot{M}(R_{\rm M})$ (e.g., Chashkina et al. 2017) as well as that of the critical luminosity (see Mushtukov et al.

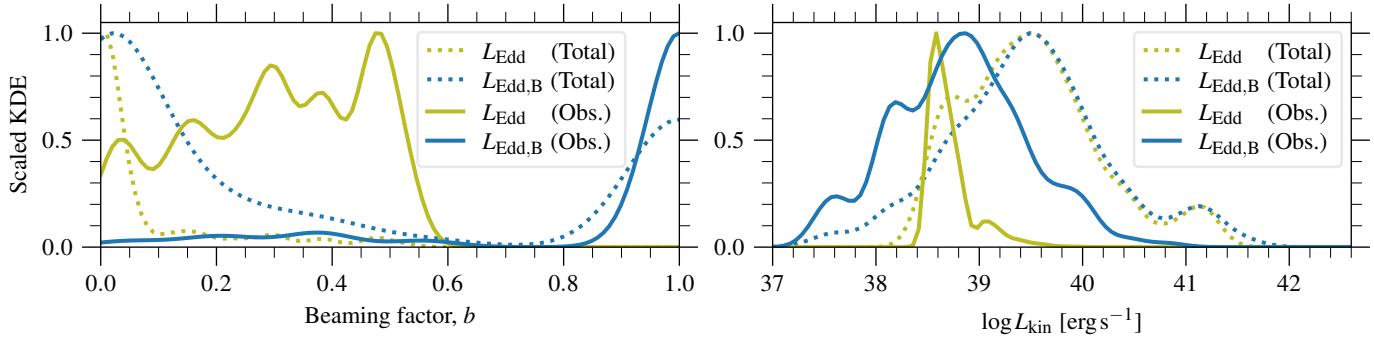

Fig. 3. Kernel density estimates (scaled to unity for visibility) of the beaming factor (left) and mechanical feedback (right) in the total (dashed) and observed (solid) population of NS-ULXs from the `POSYDON` model, using the classical (green) or modified Eddington limit (blue).

2015; Brice et al. 2021 for dipolar and multipolar fields, respectively) on the accretion geometry points at the need for prescriptions that are applicable to population synthesis models. Despite important efforts contributing to our understanding of accretion in NS-ULXs (e.g., Kuranov et al. 2020; Mushtukov et al. 2024), the effect of B in $L_{\rm Edd}$ in simulations of highly magnetised NSs remains poorly explored (see discussion in Inoue et al. 2024). In the present work, we show that this effect leads to markedly different results at the population level, even in the case where the BH-ULX prescriptions are broadly valid.

The above-mentioned improvements will enable future population synthesis codes to self-consistently model mass transfer and angular momentum loss (e.g., Misra et al. 2020), NS spin-up and disk-star coupling (e.g., Kluźniak & Rappaport 2007), and orbital evolution (e.g., Chen 2024), as well as emission and the detectability of pulsations (e.g., King & Lasota 2020). This is necessary to test models using all available data from individual ULXs and PULXs, at the population level.

Acknowledgements. We thank the anonymous referee for their valuable comments and suggestions, which have significantly improved the quality of this manuscript. KK is supported by a fellowship program at the Institute of Space Sciences (ICE-CSIC) funded by the program Unidad de Excelencia María de Maeztu CEX2020-001058-M. DM acknowledges that this project has received funding from the European Research Council (ERC) under the European Union's Horizon 2020 research and innovation programme (grant agreement No. 101002352, PI: M. Linares). RA and GLI acknowledge financial support from INAF through grant "INAF-Astronomy Fellowships in Italy 2022 – (GOG)". GLI also acknowledges support from PRIN MUR SEAWIND (2022Y2T94C), which was funded by NextGenerationEU and INAF Grant BLOSSOM.

References

Abarca, D., Parfrey, K., & Kluźniak, W. 2021, ApJ, 917, L31
Bachetti, M., Harrison, F. A., Walton, D. J., et al. 2014, Nature, 514, 202
Bachetti, M., Heida, M., Maccarone, T., et al. 2022, ApJ, 937, 125
Basko, M. M., & Sunyaev, R. A. 1976, MNRAS, 175, 395
Belfiore, A., Esposito, P., Pintore, F., et al. 2020, Nat. Astron., 4, 147
Beloborodov, A. M. 1998, MNRAS, 297, 739
Breivik, K., Coughlin, S., Zevin, M., et al. 2020, ApJ, 898, 71
Brice, N., Zane, S., Turolla, R., & Wu, K. 2021, MNRAS, 504, 701
Brightman, M., Harrison, F. A., Fürst, F., et al. 2018, Nat. Astron., 2, 312
Chashkina, A., Abolmasov, P., & Poutanen, J. 2017, MNRAS, 470, 2799
Chashkina, A., Lipunova, G., Abolmasov, P., & Poutanen, J. 2019, A&A, 626, A18
Chen, W.-C. 2024, ApJ, 973, 38
Dall'Osso, S., Perna, R., & Stella, L. 2015, MNRAS, 449, 2144
Eksi, K. Y., Andac, I. C., Cikintoglu, S., et al. 2015, MNRAS, 448, L40
El Mellah, I., Sundqvist, J. O., & Keppens, R. 2019, A&A, 622, L3
Erkut, M. H., Türkoğlu, M. M., Ekşi, K. Y., & Alpar, M. A. 2020, ApJ, 899, 97
Fragos, T., Andrews, J. J., Bavera, S. S., et al. 2023, ApJS, 264, 45
Frank, J., King, A., & Raine, D. 2002, Accretion Power in Astrophysics, 3rd edn. (Cambridge University Press)
Fürst, F., Walton, D. J., Harrison, F. A., et al. 2016, ApJ, 831, L14
Herold, H. 1979, Phys. Rev. D, 19, 2868
Inoue, A., Ohsuga, K., Takahashi, H. R., & Asahina, Y. 2023, ApJ, 952, 62
Inoue, A., Ohsuga, K., Takahashi, H. R., Asahina, Y., & Middleton, M. J. 2024, ApJ, 977, 10
Israel, G. L., Belfiore, A., Stella, L., et al. 2017, Science, 355, 817
Kaaret, P., Feng, H., & Roberts, T. P. 2017, ARA&A, 55, 303
King, A. R. 2009, MNRAS, 393, L41
King, A., & Lasota, J.-P. 2019, MNRAS, 485, 3588
King, A., & Lasota, J.-P. 2020, MNRAS, 494, 3611
King, A., & Lasota, J. P. 2021, arXiv e-prints [arXiv:2112.03779]
King, A. R., Davies, M. B., Ward, M. J., Fabbiano, G., & Elvis, M. 2001, ApJ, 552, L109
King, A., Lasota, J.-P., & Kluźniak, W. 2017, MNRAS, 468, L59
King, A., Lasota, J.-P., & Middleton, M. 2023, New Astron. Rev., 96, 101672
Kluźniak, W., & Rappaport, S. 2007, ApJ, 671, 1990
Kovlakas, K., Zezas, A., Andrews, J. J., et al. 2020, MNRAS, 498, 4790
Kovlakas, K., Zezas, A., Andrews, J. J., et al. 2021, MNRAS, 506, 1896
Kovlakas, K., Fragos, T., Schaerer, D., & Mesinger, A. 2022, A&A, 665, A28
Kuranov, A. G., Postnov, K. A., & Yungelson, L. R. 2020, Astron. Lett., 46, 658
Lasota, J.-P., & King, A. 2023, MNRAS, 526, 2506
Lehmer, B. D., Eufrasio, R. T., Basu-Zych, A., et al. 2021, ApJ, 907, 17
Lipunova, G. V. 1999, Astron. Lett., 25, 508
Liu, J. 2024, ApJ, 961, 196
Middleton, M. J., Brightman, M., Pintore, F., et al. 2019, MNRAS, 486, 2
Miller-Jones, J. C. A., Bahramian, A., Orosz, J. A., et al. 2021, Science, 371, 1046
Misra, D., Fragos, T., Tauris, T. M., Zapartas, E., & Aguilera-Dena, D. R. 2020, A&A, 642, A174
Misra, D., Kovlakas, K., Fragos, T., et al. 2023, A&A, 672, A99
Misra, D., Kovlakas, K., Fragos, T., et al. 2024, A&A, 682, A69
Mushtukov, A. A., & Portegies Zwart, S. 2023, MNRAS, 518, 5457
Mushtukov, A. A., Suleimanov, V. F., Tsygankov, S. S., & Poutanen, J. 2015, MNRAS, 454, 2539
Mushtukov, A. A., Tsygankov, S. S., Suleimanov, V. F., & Poutanen, J. 2018, MNRAS, 476, 2867
Mushtukov, A. A., Ingram, A., Middleton, M., Nagirner, D. I., & van der Klis, M. 2019, MNRAS, 484, 687
Mushtukov, A. A., Portegies Zwart, S., Tsygankov, S. S., Nagirner, D. I., & Poutanen, J. 2021, MNRAS, 501, 2424
Mushtukov, A. A., Ingram, A., Suleimanov, V. F., et al. 2024, MNRAS, 530, 730
Paczynski, B. 1992, Acta Astron., 42, 145
Pakull, M. W., & Mirioni, L. 2002, arXiv e-prints, [arXiv:astro-ph/0202488]
Paxton, B., Bildsten, L., Dotter, A., et al. 2011, ApJS, 192, 3
Pinto, C., Middleton, M. J., & Fabian, A. C. 2016, Nature, 533, 64
Poutanen, J., Lipunova, G., Fabrika, S., Butkevich, A. G., & Abolmasov, P. 2007, MNRAS, 377, 1187
Revnivtsev, M., & Mereghetti, S. 2016, in The Strongest Magnetic Fields in the Universe, eds. V. Beskin, A. Balogh, M. Falanga, et al. (New York, NY: Springer New York), 299
Shakura, N. I., & Sunyaev, R. A. 1973, A&A, 500, 33
Shapiro, S. L., & Teukolsky, S. A. 1983, Black holes, white dwarfs and neutron stars. The physics of compact objects (John Wiley & Sons, Ltd)
Vasilopoulos, G., Koliopanos, F., Haberl, F., et al. 2021, ApJ, 909, 50
Walton, D. J., Bachetti, M., Fürst, F., et al. 2018, ApJ, 857, L3
Wiktorowicz, G., Lasota, J.-P., Middleton, M., & Belczynski, K. 2019, ApJ, 875, 53
Zezas, A., Fabbiano, G., Rots, A. H., & Murray, S. S. 2002, ApJ, 577, 710

Appendix A: Analytical formulæ

Using Eqs. (1)-(6), we provide practical limits and formulæ for observed sources under the case of canonical NS mass ($1.4\,M_{\odot}$) and radius (10^6 cm). If there is evidence of beaming, then for B_{12}<0.6, ULX luminosities require $b < 0.6$. This limit increases with B until $B_{12}\approx0.9$ where b approaches unity. In the weak B case, the beaming factor can be constrained by the apparent luminosity (solving eq. 6 in Kovlakas et al. 2022 for b):

$$b_{\rm min} \approx \left(5.5{\times}10^{38}\,{\rm erg\,s^{-1}}/L_{\rm iso}\right)^{8/9}. \tag{A.1}$$

Evidence of beaming exceeding this value ($b_{\rm min}$<b<1) can be used to estimate the B:

$$B_{12} = \left[\frac{bL_{\rm iso}}{3.5{\times}10^{38}\,{\rm erg\,s^{-1}}\,(3.14 + \ln b^{-1/2})}\right]^{3/4}, \tag{A.2}$$

whereas, lack of beaming puts a lower limit on the B,

$$B_{12} > \left(L_{\rm iso}/1.1{\times}10^{39}\,{\rm erg\,s^{-1}}\right)^{3/4}. \tag{A.3}$$